Annals of Data Science
https://doi.org/10.1007/s40745-022-00436-2

High Resolution Solar Image Generation Using Generative Adversarial Networks

Ankan Dash[1] · Junyi Ye[1] · Guiling Wang[1] · Huiran Jin[2]

Received: 1 February 2022 / Revised: 7 June 2022 / Accepted: 10 June 2022

Abstract

We applied Deep Learning algorithm known as Generative Adversarial Networks (GANs) to perform solar image-to-image translation. That is, from Solar Dynamics Observatory (SDO)/Helioseismic and Magnetic Imager (HMI) line of sight magnetogram images to SDO/Atmospheric Imaging Assembly (AIA) 0304-Å images. The Ultraviolet (UV)/Extreme Ultraviolet observations like the SDO/AIA 0304-Å images were only made available to scientists in the late 1990s even though the magnetic field observations like the SDO/HMI have been available since the 1970s. Therefore, by leveraging Deep Learning algorithms like GANs we can give scientists access to complete datasets for analysis. For generating high resolution solar images, we use the Pix2PixHD and Pix2Pix algorithms. The Pix2PixHD algorithm was specifically designed for high resolution image generation tasks, and the Pix2Pix algorithm is by far the most widely used image to image translation algorithm. For training and testing we used the data for the year 2012, 2013 and 2014. After model training, we evaluated the model on the test data. The results show that our deep learning models are capable of generating high resolution (1024×1024 pixels) SDO/AIA0304 images from SDO/HMI line of sight magnetograms. Specifically, the pixel-to-pixel Pearson Correlation Coefficient of the images generated by Pix2PixHD and original images is as high as 0.99. The number is 0.962 if Pix2Pix is used to generate images. The results we get for our Pix2PixHD model is better than the results obtained by previous works

✉ Ankan Dash
ad892@njit.edu

Junyi Ye
jy394@njit.edu

Guiling Wang
guiling.wang@njit.edu

Huiran Jin
hrjin@njit.edu

[1] Department of Computer Science, New Jersey Institute of Technology, Newark, NJ 07102, USA

[2] School of Applied Engineering and Technology, New Jersey Institute of Technology, Newark, NJ 07102, USA

Published online: 02 August 2022

done by others to generate SDO/AIA 0304 images. Thus, we can use these models to generate AIA0304 images when the AIA0304 data is not available which can be used for understanding space weather and giving researchers the capability to predict solar events such as Solar Flares and Coronal Mass Ejections. As far as we know, our work is the first attempt to leverage Pix2PixHD algorithm for SDO/HMI to SDO/AIA0304 image-to-image translation.

Keywords Solar images · Deep learning · Generative adversarial networks · Image processing

1 Introduction

The sun is the main source of space weather due to its constant emission of energy and electromagnetic radiation in the form of light and electrically charged particles [1]. Several solar phenomena like Solar Flares, Coronal Mass Ejections (CMEs), High Speed solar winds and Solar energetic particles constitute the solar weather and cause space weather effects here on Earth [2]. Solar Flares are giant bursts of energy and radiations comprising of X-Rays and Gamma Rays due to the sudden release of magnetic energy that has built up in the solar atmosphere [3]. Coronal Mass Ejections (CME) are giant clouds of magnetic plasma in the Sun's corona that are hurled into space. CMEs can generate strong shock-waves that can accelerate solar wind and extend billions of miles into space [4]. The regions of the Sun known as coronal holes produce high-speed solar wind streams [5]. Solar energy particles are high-energy particles from the Sun that can come either from the site of a solar flare or from shock waves associated with coronal mass ejections [6]. It is extremely important to have the capabilities to predict the above solar events because astronauts run the risk of being exposed to solar radiation. Also, these solar events can interfere with proper functioning of satellites and cause power grid disruption which will be a major problem in today's digitally connected world [7].

To give scientists and researchers prediction capabilities, NASA and several other Space organizations across the globe are constantly monitoring the Sun's activities. Numerous space missions like the Solar Heliospheric Observatory (SOHO) [8], Solar Terrestrial Relations Observatory (STEREO) [9] and Solar Dynamics Observatory (SDO) [10] capture various observations of the Sun at different wavelengths which include the Ultraviolet (UV), Extreme Ultraviolet (EUV) images, solar magnetograms and dopplergrams. The NASA Living With a Star (LWS) [11] is a program whose primary objective is to study the Sun and its effects on the Earth. The Solar Dynamics Observatory (SDO) is the first mission launched by NASA under the LWS program. The SDO takes high resolution images of the Sun at various wavelengths to help solar physicists understand the generation and the structure of the Sun's magnetic field, and to have predictive capability of events like Solar Flares and Coronal Mass Ejections (CMEs). The SDO contains a variety of instruments like HMI (Helioseismic and Magnetic Imager) [12], AIA (Atmospheric Imaging Assembly) [13] and EVE (Extreme Ultraviolet Variability Experiment) [14] to capture various observations of the Sun. The HMI instrument is led by Stanford University and focuses on the movement and

magnetic properties of the sun's surface and provides 3 images. Managed by the Lockheed Martin Solar and Astrophysics Laboratory (LMSAL), the AIA instrument takes continuous full-disk observations of the solar chromosphere and corona at 10 different wavelengths measured in angstroms (Å). The EVE instrument is led by University of Colorado and measures the EUV irradiance.

Researchers now have access to information that was previously difficult to obtain due to the availability of vast amounts of data. Data science is a field of study that deals with large amounts of data and uses cutting-edge tools and procedures to uncover hidden patterns and derive useful information. Preparing data for analysis and processing, performing advanced data analysis, and presenting the results to identify patterns are all part of data science and big data [15]. Data science is a broad term that encompasses a variety of operations including data mining, machine learning, deep learning, and artificial intelligence [16]. With the advent of big data and advanced Machine Learning [17] and Deep Learning algorithms, we can now tackle some of the complex and challenging problems in a wide variety of domains [18, 19].

Deep Learning [20] has been revolutionizing many fields, from self-driving cars to medicine and it was only a matter of time before it found its way into physical sciences. Generative Adversarial Networks [21] or GANs for short are a type of generative models that were invented by Ian Goodfellow and his colleagues. Generative Models [22] try to learn a probability density function from a training set and then generate new samples that are drawn from the same distribution. Some of these models include Boltzmann Machines [23], Deep Belief Networks [24] and Variational Autoencoders [25]. Generative Adversarial Networks [21] are by far the most widely used generative models. GANs work by pitting two neural networks (the Generator and the Discriminator) against each other to generate new synthetic images that are like the real images. Over the past couple of years, GANs have made significant progress. With the increase in model capacity, we are now able to train deeper and more complex Generator and Discriminator neural network architectures due to hardware improvements. GAN variations such as Progressive GAN [26] enable us to generate high resolution images with improved training stability. Paired image-to-image translation GANs (Pix2Pix [27]) and unpaired image-to-image translation GANs (CycleGAN [28]) can find a mapping between paired and unpaired pairs of images to solve the image-to-image translation problems. Even though Pix2Pix has been widely used for image translation (Kim et al. [29], Park et al. [30]) tasks, it is not well suited for the generation of high-resolution images and it fails to capture finer details and can sometime cause artifacts in high resolution image to image translation tasks. To overcome this problem the Pix2PixHD algorithm proposed by Wang et al. [31] can be used to generate high-res images with minimum artifacts and capture finer details of the image.

1.1 Motivation

The UV/EUV observations like the ones taken by the SDO/AIA instrument were only made available after the launch of the SOHO observatory in the late 1990s. However, the magnetic field observations like the ones captured by the SDO/HMI instrument have been available since the 1970s. UV and EUV observations which include the

AIA0304 measurements help researchers to understand different areas of the sun, such as coronal loops, filaments, coronal holes, active regions [32] and are thus vital in space weather prediction.

Even though there have been some attempts for solar image generation using deep learning [29, 30, 33–35], most of them have focused on the generation of Solar Farside Magnetograms or Magnetic Field observations from UV and EUV data [29, 34, 35] but very few have tried to generate UV and EUV images using magnetograms [30]. Also, most of the works related to the generation of UV and EUV images from magnetograms have been using the Pix2Pix algorithm [30].

In this work we implemented conditional Generative Adversarial Networks, to perform image-to-image translation. More specifically, we use the Pix2PixHD and the Pix2Pix models to generate high resolution SDO/AIA0304 images from SDO/HMI line of sight magnetograms.

Here we have considered only the AIA-304 Å passband out of the 9 passbands (94, 131, 171, 193, 211, 304, 335, 1600, and 1700 Å). This is because the magnetic fields themselves are invisible but as the charged plasma moves along the magnetic field lines these magnetic fields become visible at the extreme ultraviolet wavelength of 304 Å, showing material at a temperature of approximately 50,000 Kelvin. This allows scientists to observe and analyze the magnetic fields on the sun. Despite the fact that we have focused on generating AIA0304 images using HMI images, this framework is compatible with the other passbands and can be used to create high-quality images for any of the other 9 passbands. Aside from that, our approach may also be utilized to translate AIA images to HMI images. As a result, the models can do image to image translation in either direction.

Thus, by using GANs we generate AIA0304 images using HMI images when the AIA0304 images are not available to scientists. In this way we can provide scientists and researchers access to complete solar magnetogram and UV/EUV data.

1.2 Motivation

In this section the major contributions of this work are highlighted:

- As far as we know, our work is the first attempt to leverage Pix2PixHD algorithm for SDO/HMI to SDO/AIA0304 image-to-image translation and we have shown that Pix2PixHD can indeed be used to solve such problems. The results (Relative Error: -0.045, Pixel to Pixel Pearson correlation coefficient: 0.99, PPE10 or percentage of pixels with relative error less than 10 percent: 0.823 and Structural Similarity Index Measure: 0.96) indicate that GANs can be extremely useful in generating AIA0304 images from SDO/HMI images. The Pix2PixHD algorithm is able to learn complex features and fine details during training and then reproduce them during testing.
- We have modified the original Pix2PixHD algorithm to solve our task, since the original Pix2PixHD algorithm was designed to synthesize high-resolution images from semantic label maps using conditional generative adversarial networks, while we have employed the Pix2PixHD algorithm for our paired image-to-image translation task.

- We also have modified and implemented the Pix2Pix algorithm to serve as the benchmark model. We have modified the original Pix2Pix algorithm to be able to generate high resolution images. To do this we modified the Generator's neural network architecture.
- Our Pix2PixHD model outperforms the Pix2Pix benchmark model and the previously implemented models by a substantial amount. Our model was trained using only 1892 images, which indicates the effectiveness of our model in small data sets.

2 Related Work

Galvez et al. [33] used Convolutional Neural Networks or CNN [36] to map three channel 256 × 256 HMI images to 9 channel 256 × 256 AIA images. Park et al. [30] applied deep learning for paired image to image translation from solar magnetograms to solar UV and EUV images. To do this they considered two CNN models with two different loss functions one with just L1 loss (L1) and the other with L1 plus the cGAN loss (LcGAN). Kim et al. [29] used cGAN [27] to generate solar farside magnetograms from STEREO/Extreme UltraViolet Imager (EUVI) 304- Å images. For this they used pairs of SDO/AIA0304 images and SDO/HMI magnetograms to train their deep learning model and then generated solar farside magnetograms using the STEREO/Extreme UltraViolet Imager (EUVI) 304 images. Shin et al. [34] used the Pix2PixHD model to generate high resolution magnetograms from Ca II K images. They used pairs of Ca II K 393.3 nm images from the Precision Solar Photometric Telescope at the Rome Observatory [37] and SDO/HMI line-of-sight magnetograms to train their model. Jeong et al. [35] used pairs of SDO/AIA three passband (304, 193, and, 171) images and the SDO/HMI LOS 720 s magnetograms to train their Pix2PixHD model and then generate solar farside magnetograms using the STEREO/EUVI A and B (304, 195, and 171 Å) passband images.

3 Data and Methodology

In this section we describe about the Data and the Method used. The Data subsection provides description about the data source, file format, processing and preparation for deep learning application. The Methods subsection includes details about the model's architecture, the loss function, model training and evaluation framework used.

3.1 Data

The datasets used is available on the Joint Science Operations Center (JSOC) server where the Solar Dynamics Observatory (SDO) data can be found. To get the data, perform image processing and prepare the data for the deep learning we used Python packages like SunPy and Astropy. The data are available in Flexible Image Transport System (FITS) file format which is the most extensively used digital file format for storing astronomical data. The FITS file contains metadata which are vital for image

processing, visualization and analysis. The AIA0304 and HMI images were extracted from their FITS files respectively. Aligning, rotating, centering and converting to 1024 $\times$ 1024 RGB images was carried out. The above image processing steps are based on relevant domain knowledge and can be followed to replicate the results using Python packages like SunPy and Astropy. Some of the images with poor quality, excessive noise due to solar flares and obstruction because of planetary transit were manually removed. For model training we are using data for the year 2012, 2013 and 2014 excluding the data for October, November and December of the year 2014 which are used for model testing. This gives us a total of 1892 HMI-AIA0304 image pairs for model training and 200 image pairs for testing and evaluation. We did not include the data for the subsequent years due to hardware constraints and due to the subsequent degradation of the SDO/AIA0304-Å instrument which results in loss of details captured in the images.

3.2 Methods

The following section describes the Pix2Pix and the Pix2PixHD neural network architecture along with the objective or the loss function used, the model training process and the model evaluation metrics used to quantify the model's performance.

We're using the Pix2Pix and Pix2PixHD models since we're doing paired image to image translations, which the Pix2Pix and Pix2PixHD models were designed for. This is due to the fact that each pair of images is related and cannot be viewed as a distinct entity. There is other image to image translation models such as CycleGAN [28] and StarGAN [38]. However, they are not suitable for our task for the following reason. CycleGAN is used for unpaired image to image translation where there are no correlations between the pairs of images. StarGAN is used for image-to-image translation for multiple domains. For example, we have 1 input image and we have more than 1 output images. However, our case is pairwise translation and thus, we do not use StarGAN for our task.

3.3 Pix2Pix Network Architecture, Objective Function and Model Training

3.3.1 Network Architecture

The algorithm used is the conditional image-to-image translation Generative Adversarial Network, cGAN [27]. Since the original Pix2Pix algorithm was not designed to generate high resolution images, we have modified the original algorithm to handle 1024 $\times$ 1024, 3 channel RGB solar images. The modifications include adding additional layers to the U-Net [39] architecture which is described below. The GAN consists of a Generator which has a U-Net [39] architecture and the Discriminator is a PatchGAN [27] classifier. To handle 1024 $\times$ 1024 images, in our algorithm the Generator contains 10 encoder and decoder blocks respectively. Each encoder blocks consisting of Convolutional layers, Batch Normalization and LeakyReLU activations while each decoder blocks are consisting of Transposed convolutions, Batch Normalization, ReLU activations. The U-Net also contains skip connections that concatenate

the encoder and the decoder blocks at the same resolution to prevent loss of important information during the forward pass for the encoding stage and also help in improving the flow of gradients back to the encoder during the backward pass, preventing the problem of vanishing gradients. Dropout layers are also used in some blocks to incorporate stochasticity into the network during training. The Discriminator is a PatchGAN. A PatchGAN is a CNN that tries to classify patches of an image as real or fake, rather than the whole image. The output of a PatchGAN a matrix (2d-array), instead of just a single value. PatchGAN consists of Convolutional layers, Batch Normalizations and LeakyReLU activations.

3.3.2 Objective Function

The objective or the loss function for the Discriminator is the traditional adversarial loss function, that is the negative log likelihood minimization for recognizing fake and ground truth images conditioned on the ground truth image. The Generator on the other hand is trained using the adversarial loss along with the L1 or pixel distance loss between the generated image and the real or target image. The L1 loss encourages the generated image for a particular input to remain as similar as possible to the corresponding output real or ground truth image. This leads to faster convergence and more stable training. The loss function for conditional GAN is given by

$$L_{cGAN}(g, d) = E_{x,y}[\log d(x, y)] + E_x[\log(1 - d(x, g(x))], \tag{1}$$

where the generator g tries to minimize the above function whereas the discriminator d tries to maximize it. In the above equation x is the input, y is ground truth, $g(x)$ is the generated fake output. The above equation can also be written as

$$g^* = \min_g \max_d L_{cGAN}(g, d) \tag{2}$$

The $L1$ loss or the pixel distance loss is given by

$$L_1 = E_{x,y}(\|y - g(x)\|_1) \tag{3}$$

The goal of the generator is to minimize the above pixel distance loss term hence the final loss/objective can be written as

$$g^* = \min_g \max_d L_{cGAN}(g, d) + \lambda L_1(g) \tag{4}$$

where λ is the weighting hyper-parameter coefficient. In our case we took $\lambda = 100$ similar to the what was used by [27].

3.3.3 Pix2Pix Model Training

During training the goal of the Generator which has a U-Net architecture is to take in as input SDO/HMI images and then generate images that look like the real

SDO/AIA0304. The generator tries to minimize the conditional GAN loss (LcGAN) along with the pixel distance (L_1) loss. The discriminator on the other hand tries to determine which ones are the real pairs of SDO/AIA0304, SDO/HMI images and which are the generated (fake) pairs by minimizing the adversarial loss. Figure 1 shows the working of the Pix2Pix image-to-image translation conditional GAN model.

Both the real and the generated AIA0304 images are concatenated with SDO/HMI images respectively along the channel dimension to form the real and generated pairs of images. The Discriminator which is a PatchGAN, attempts to identify which one is the real pair and which one is the fake/generated pair by outputting a matrix of values between 0 and 1 which shows how real of how fake different parts of the image are. We picked a batch size of 1 to train the model because it has been shown to be effective at image production tasks in the original Pix2Pix paper. The optimizer used is Adam with a learning rate of 0.0002, β_1 set to 0.5 and β_2 set to 0.009. Our model was trained for 200 epochs on Google Colab Pro with GPU acceleration. For every 10 epochs the generator model was saved for making predictions after model training. This gives us a total of 20 generator models from which we can choose the best model during model evaluation on the unseen test data.

3.4 Pix2PixHD Network Architecture, Objective Function and Model Training

3.4.1 Network Architecture

The Pix2PixHD [31] is an improved version of the Pix2Pix algorithm. The primary goal of Pix2PixHD is to produce high-resolution images. To do this the authors introduced multi-scale generators and discriminators. Pix2PixHD conditional GAN consists of a Coarse to Fine Generator which has two components, the Global generator G1 and the Local enhancer G2. There is no difference between G1 and the Pix2Pix generator, it is an end2end U-Net structure. The Global generator G1 is made up of 3 components that include a convolutional front-end (encoder), a set of residual blocks and a transposed convolutional back-end (decoder). The local enhancer is made up of 3 components which include a convolutional front-end, a set of residual blocks and a transposed convolutional back-end. The global generator is sandwiched between two halves of the G2 generator. The left half of G2 extracts features, fuses them with the previous layer features of G1's output layer, and sends the resulting information to the right half of G2 to produce a high-resolution image. The network architecture of the discriminator remains unchanged from the Pix2Pix algorithm, i.e., a patch based fully connected convolutional neural network. What changes is that we no longer just use one discriminator instead we use multiple (in our case two) discriminators that operate at different scales. Having two discriminators operating at different scales encourages the generator to produce images that are consistent globally without lacking the local finer details.

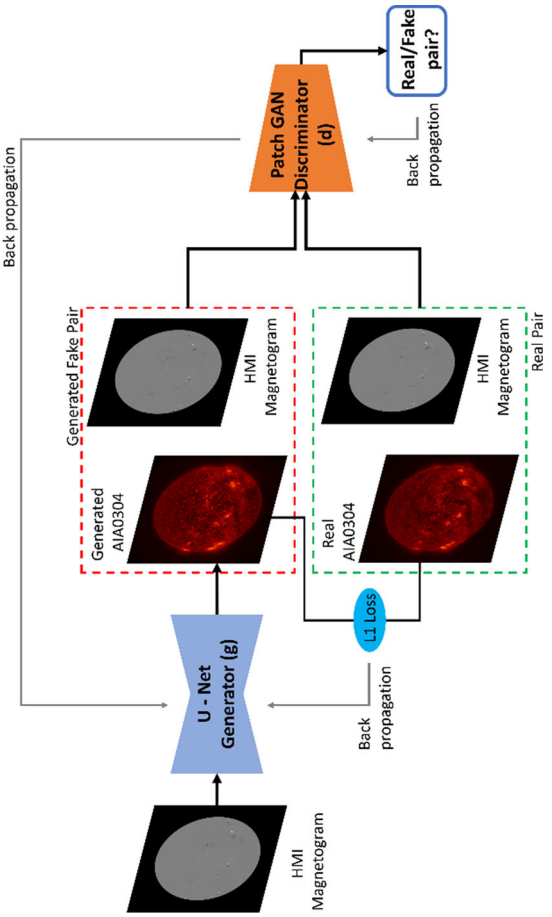

Fig. 1 Pix2Pix Conditional GAN model for paired image-to-image translation

3.4.2 Objective Function

The authors of Pix2PixHD improved upon the traditional conditional GAN loss by incorporating the Feature matching loss LFM based on the discriminator. We have already described the LcGAN loss in the previous section. The feature matching loss acts as regularization and stabilizes training as the generator now has to produce similar statistics at multiple scales. The feature matching loss is given by

$$L_{FM}(g, d) = E_{x,y} \sum_{i=1}^{T} \left[\| d^i(x, y) - d^i(x, g(x) \|_1 \right] \tag{5}$$

where T is the total number of layers, i is the serial number of the layers and N_i represents the number of pixels in each layer. The objective function is given by

$$\min_{g} \left(\left(\max_{d_1, d_2} \sum_{k=1,2} L_{cGAN}(g, d_k) \right) \right) + \lambda \sum_{k=1,2} L_{FM}(g, d_k) \Bigg) \Bigg) \tag{6}$$

where k denotes the serial number of the two discriminator and λ denotes the weighting hyperparameter. We use the value of λ to be 10 which was used by Pix2PixHD [31] model.

3.4.3 Pix2Pix Model Training

Similar to the training of the Pix2Pix algorithm described above. Figure 2 shows the working of the Pix2PixHD image-to-image translation conditional GAN model. During training of the Pix2PixHD model, the input is the HMI image and the output is the generated AIA304 image. The network then updated the parameters based on the calculated values of the LcGAN and the LFM. We train the model for 200 epochs and saved the generator model every 10 epochs for testing on the test data. Similar to the Pix2Pix model, a batch size of 1 was used. We used the Adam optimizer with learning rate of 0.0002, β_1 equals to 0.5 and β_2 equals to 0.999.

3.5 GAN Training Convergence

GAN models often do not converge; instead, an equilibrium between the generator and discriminator models is found. In general, a GAN is said to have converged when both the generator and discriminator losses have converged to a stable value. The loss of the generator grows as the discriminator improves, until they both stabilize and the entire GAN is said to have converged. Determining when to quit training is generally difficult. In this paper, we preserve the model at regular intervals (every 10 epochs) throughout training to find the best model through testing. We monitor the losses for the generators and discriminators for both the models to determine when to stop training. For both the Pix2Pix and the Pix2PixHD model, we found the losses for the generator and the discriminators stabilized and converged after 200 epochs.

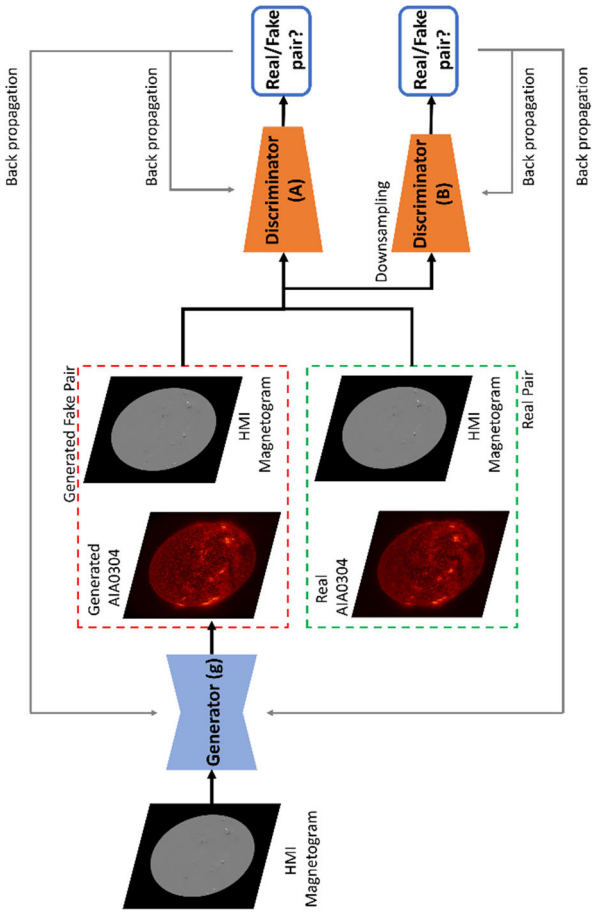

Fig. 2 Pix2PixHD GAN model for paired image-to-image translation

3.6 Model Evaluation

To quantify the model's performance and compare the real SDO/AIA0304 images with the GAN generated ones for the entire test dataset we used the following four types of evaluation metrics.

The first model evaluation metric is the Relative Error (RE). Relative error of the total pixel value (Φ_i) is given by

$$RE_i = \frac{abs\left(\Phi_i^{GAN} - \Phi_i^{AIA0304}\right)}{\Phi_i^{AIA0304}} \tag{7}$$

where i represents the serial number of the 200 testing image data samples. Lower absolute value of relative indicates better performance.

The second metric for evaluation is the Pixel-to-Pixel Pearson Correlation Coefficient (CC). A higher value of CC denotes that the GAN model is not only able to generate the correct pixel values but also the values are spatially correct.

The third metric is the Percentage of Pixel Having Relative Error Less than 10% (PPE10) which finds the fraction of the number of pixels in an image which have relative error less than 10% and indicates the percentage of good pixels in the generated image. Higher PPE10 value indicates better performance.

The final model evaluation metric is the Structural similarity index measure (SSIM) [40] which is a method for quantifying the similarity between two images. SSIM tries to model the perceived change in the image's structural information. The SSIM value varies between -1 and 1, where a value of 1 shows perfect similarity and a higher value indicates better performance.

4 Results and Discussion

From Fig. 3, we can see the SDO/HMI magnetogram images as input along with the ground truth SDO/AIA0304 images and the Pix2PixHD generated AIA0304 images. In the figure we can observe that the Pix2PixHD model learns the active region and quiet region patterns for the full disc during training and then is able to generate these regions during testing/image generation step. The Pix2PixHD generated images are of high quality and are comparable to the real images.

Table 1 presents the evaluation metric values for the entire test dataset consisting of 200 images for the month of September, October, November and December for the year 2014. We compare the results of the our Pix2PixHD model and Pix2Pix model with the baseline model trained using the algorithm developed by [30].

From Table 1. we can observe that our Pix2Pix model and Pix2PixHD model are able to get better results than the results obtained by utilizing the model trained using [30] algorithm on our test dataset. The Pix2PixHD model outperforms all the other models. The relative error of -0.045 suggests that the Pix2PixHD model Generator underestimates the pixel values slightly while the Pix2Pix models overestimate the pixel values. The Pixel-to-pixel Pearson correlation co-efficient (PCC) value of 0.99 for Pix2PixHD indicates strong linear relation between the generated and the real

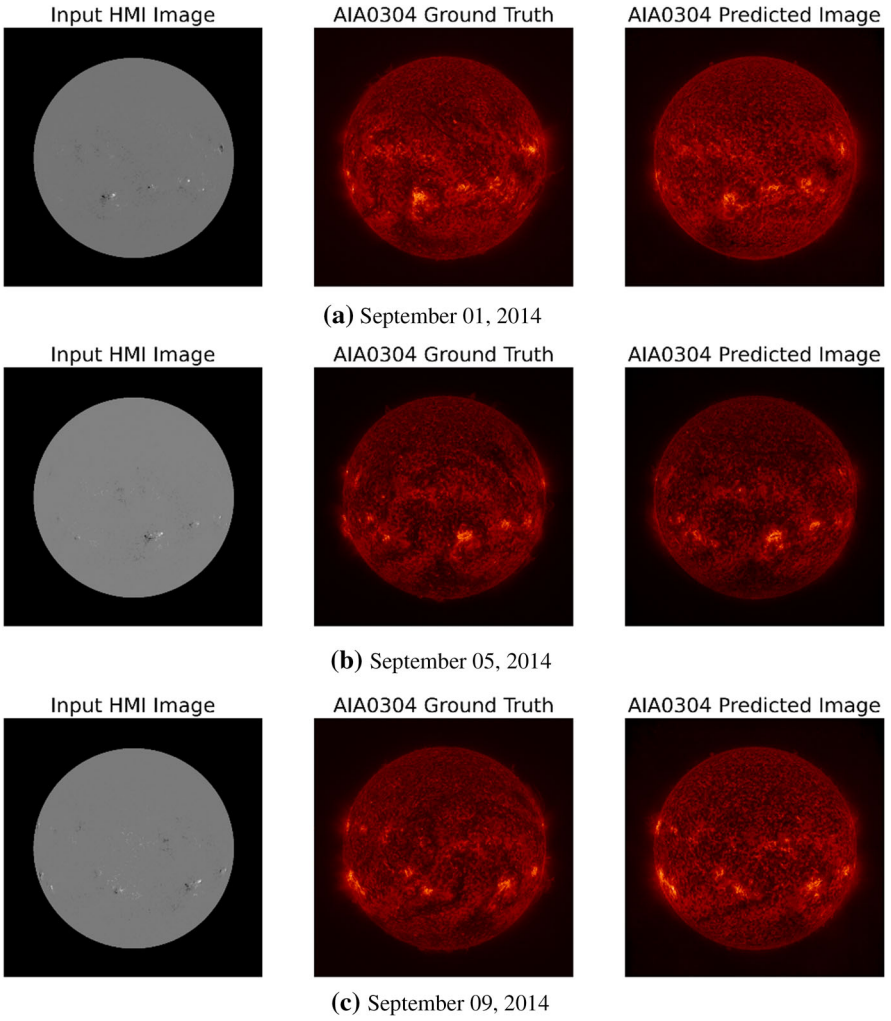

Fig. 3 Comparison between real AIA0304 and Pix2PixHD cGAN generated ones. **a**–**c** show the input HMI image, the ground truth AIA0304 image and the GAN generated AIA0304 images respectively taken for the month of September with 4-day cadence

images. The other algorithm used by Park et al. performs slightly less than our Pix2Pix model. The Pix2PixHD algorithm also does much better than the other algorithms with more than 14% increase for the PPE10 values, this shows the Pix2PixHD model makes less than 10% error on much higher number of pixels when compared to other models. Finally, the SSIM value of 0.96 for the Pix2PixHD model demonstrates that it is able to learn and generate intricate structures in the images. The algorithm used by [30] is also based upon the Pix2Pix algorithm therefore the performance is similar though slightly lower than our Pix2Pix model which indicate that the modifications we made to the original Pix2Pix algorithm helps our model to achieve slight improvement over

Table 1 Model Evaluation metrics for Pix2PixHD and Pix2Pix generated images for the full disk. Comparing results with Park et al. [30]

Metrics	Full disk 200 Images		
	Pix2Pix2Pix (ours)	Pix2Pix (ours)	Park et al. [30]
Relative error (RE)	−0.045	0.055	0.061
Pixel-to-pixel Pearson correlation coefficient (PCC)	0.99	0.962	0.933
Percentage of pixel having error less than 10% (PPE10)	0.823	0.681	0.652
Structural Similarity Index measure (SSIM)	0.96	0.884	0.851

previously implemented models. Thus, by implementing the Pix2Pix model we prove that the Pix2Pix, which is the benchmark image to image translation algorithm is also able to learn the structures of the images and obtain reasonable values. However, the Pix2PixHD model clearly surpasses our Pix2Pix model and all other previous works in generating high-resolution images. This can be attributed to the fact that instead of using single Generator and Discriminator architecture similar the Pix2Pix algorithm, Pix2PixHD algorithm uses a multi-scale network structure for the Generator and the Discriminator which helps to stabilize training, generate high resolution and vivid images. Also, the addition of the feature matching loss helps to stabilize model training, improve image resolution, color and texture.

The above results show that the Pix2PixHD model can successfully generate SDO/AIA0304 images from SDO/HMI magnetograms. Note that our Generative Adversarial model was trained using just 1892 images the results that we got are promising. Typically, other deep learning algorithms such as CNNs generally require copious amounts of data to identify patterns in the images and solve similar image-to-image translation problems.

5 Conclusion and Future Work

Here we used the conditional Generative Adversarial Network framework (Pix2PixHD) to perform image-to-image translation, from SDO/HMI images to SDO/AIA0304 images. As far as we know, this is the first time the Pix2PixHD algorithm has been used for SDO/HMI to SDO/AIA0304 image-to image-translation and we have shown that Pix2PixHD can indeed be used to solve such problems. The results (Relative Error: -0.045, Pixel to Pixel Pearson correlation coefficient: 0.99, PPE10 or percentage of pixels with relative error less than 10%: 0.823 and Structural Similarity Index Measure: 0.96) indicate that GANs can be extremely useful in generating AIA0304 images from SDO/HMI images. The Pix2PixHD algorithm is able to learn complex features and fine details during training and then reproduce them during testing. We used data for the year 2012, 2013 and 2014 for model training excluding the data for October, November and December of the year 2014 which were used for

model testing. The choice for the amount of data used was governed by hardware constraints and degradation of the SDO/AIA0304 instrument. In the future iteration we plan to use the data for the subsequent years by applying degradation correction factor to account for the degradation of AIA0304-˚A instrument. Since the data are temporally and spatially oriented the use of Video-to-Video Synthesis models like Vid2Vid can also be explored.

Author contributions The project's creation involved input from every author. Ankan Dash conceptualized the problem statement, collected the data, and carried out the analysis. Ankan Dash, Junyi Ye, Guiling Wang, and Huiran Jin wrote the manuscript's first draft. All authors provided feedback on earlier drafts of the work. The final manuscript was read and approved by all writers.

Funding No funding was received for this work.

Data availability The datasets used are available on the Joint Science Operations Center (JSOC) where the Solar Dynamics Observatory (SDO) data can be found. http://jsoc.stanford.edu/.

Code availability https://github.com/ankan2709/Image-Generation-Using-GANs.

Declarations

Conflict of interest The authors have no conflict of interests.

Ethical statements We hereby declare that this manuscript is the result of our independent creation under the reviewers' comments. Except for the quoted contents, this manuscript does not contain any research achievements that have been published or written by other individuals or groups. We are the sole authors of the manuscript. The legal responsibility of this statement shall be borne by us.

References

1. Solar Storm and Space Weather. https://www.nasa.gov/missionpages/sunearth/spaceweather/index.html. Accessed 27 Jan 2021
2. Echer E, Gonzalez WD, Guarnieri FL, Lago AD, Vieira LEA (2005) Introduction to space weather. Adv Space Res 35(5):855–865. https://doi.org/10.1016/j.asr.2005.02.098. FundamentalsofSpaceEnvironmentScience
3. Fletcher L, Dennis BR, Hudson HS, Krucker S, Phillips K, Veronig A, Battaglia M, Bone L, Caspi A, Chen Q et al (2011) An observational overview of solar flares. Space Sci Rev 159(1–4):19–106. https://doi.org/10.1007/s11214-010-9701-8
4. Forbes TG (2000) A review on the genesis of coronal mass ejections. J Geophys Res 105(10):23153–23165. https://doi.org/10.1029/2000JA000005
5. Garton TM, Murray SA, Gallagher PT (2018) Expansion of high-speed solar wind streams from coronal holes through the inner heliosphere. Astrophys J 869(1):12. https://doi.org/10.3847/2041-8213/aaf39a
6. Reames DV (2020) Solar energetic particles (Second Edition)
7. Marov MY et al (2014) Solar flares and impact on earth. In: Allahdadi F, Pelton J (eds) handbook of cosmic hazards and planetary defense. Springer, Cham
8. Domingo V, Fleck B, Poland AI (1995) The soho mission: an overview. Sol Phys 162(1):1–37. https://doi.org/10.1007/BF00733425
9. Kaiser ML, Kucera TA, Davila JM et al (2008) The stereo mission: an introduction. Space Sci Rev 136(1):5–16
10. Pesnell WD, Thompson BJ, Chamberlin PC (2012) The solar dynamics observatory (sdo). Solar Phys 275(1):3–15. https://doi.org/10.1007/s11207-011-9841-3

11. Brewer DA, Barth JL, Label KA, Kauffman WJ, Giffin G (2002) Nasa's living with a star program: science with relevance. Acta Astronaut 51(1):609–616. https://doi.org/10.1016/S0094-5765(02)00053-X
12. Scherrer PH, Schou J, Bush RI, Kosovichev AG, Bogart RS, Hoeksema JT, Liu Y, Duvall TL, Zhao J, Title AM, Schrijver CJ, Tarbell TD, Tomczyk S (2012) The helioseismic and magnetic imager (hmi) investigation for the solar dynamics observatory (sdo). Sol Phys 275(1):207–227. https://doi.org/10.1007/s11207-011-9834-2
13. Lemen JR, Title AM, Akin DJ, Boerner PF, Chou C, Drake JF, Duncan DW, Edwards CG, Friedlaender FM, Heyman GF, Hurlburt NE, Katz NL, Kushner GD, Levay M, Lindgren RW, Mathur DP, McFeaters EL, Mitchell S, Rehse RA, Schrijver CJ, Springer LA, Stern RA, Tarbell TD, Wuelser J-P, Wolfson CJ, Yanari C, Bookbinder JA, Cheimets PN, Caldwell D, Deluca EE, Gates R, Golub L, Park S, Podgorski WA, Bush RI, Scherrer PH, Gummin MA, Smith P, Auker G, Jerram P, Pool P, Soufli R, Windt DL, Beardsley S, Clapp M, Lang J, Waltham N (2012) The atmospheric imaging assembly (aia) on the solar dynamics observatory (sdo). Sol Phys 275(1):17–40. https://doi.org/10.1007/s11207-011-9776-8
14. Woods TN, Eparvier FG, Hock R, Jones AR, Woodraska D, Judge D, Didkovsky L, Lean J, Mariska J, Warren H, McMullin D, Chamberlin P, Berthiaume G, Bailey S, Fuller-Rowell T, Sojka J, Tobiska WK, Viereck R (2012) Extreme ultraviolet variability experiment (eve) on the solar dynamics observatory (sdo): Overview of science objectives, instrument design, data products, and model developments. Sol Phys 275(1):115–143. https://doi.org/10.1007/s11207-009-9487-6
15. Shi Y (2022) Advances in big data analytics: Theory. algorithms and practices. Springer, Berlin
16. Olson DL, Shi Y (2006) Introduction to Business Data Mining. McGraw Hill Higher Education, Maidenhead
17. Shi Y, Tian Y-J, Kou G, Peng Y, Li J (2011) Optimization based data mining: theory and applications. In: Advanced information and knowledge processing
18. Teixeira Zavadzki de Pauli S, Kleina M, Bonat WH (2020) Comparing artificial neural network architectures for brazilian stock market prediction. Ann Data Sci 7(4):613–628. https://doi.org/10.1007/s40745-020-00305-w
19. Tien JM (2017) Internet of things, real-time decision making, and artificial intelligence. Ann Data Sci 4(2):149–178. https://doi.org/10.1007/s40745-017-0112-5
20. LeCun Y, Bengio Y, Hinton G (2015) Deep learning. Nature 521(7553):436–444. https://doi.org/10.1038/nature14539
21. Goodfellow I, Pouget-Abadie J, Mirza M, Xu B, Warde-Farley D, Ozair S, Courville A, Bengio Y (2014) Generative adversarial nets. In: Ghahramani Z, Welling M, Cortes C, Lawrence N, Weinberger KQ (eds) Advances in neural information processing systems, vol 27, pp 2672–2680. Curran Associates Inc, New York
22. Harshvardhan GM, Gourisaria MK, Pandey M, Rautaray SS (2020) A comprehensive survey and analysis of generative models in machine learning. Comput Sci Rev 38:1085. https://doi.org/10.1016/j.cosrev.2020.100285
23. Hinton G (2010) Boltzmann machines. In: Sammut C, Webb GI (eds) Encyclopedia of machine learning. Springer, Boston, MA, pp 132–136
24. Hinton G (2010) Deep belief nets. In: Sammut C, Webb GI (eds) Encyclopedia of machine learning, pp 267–269. Springer, Boston, MA
25. Kingma DP, Welling M (2014) Auto-encoding variational bayes
26. Karras T, Aila T, Laine S, Lehtinen J (2018) Progressive growing of GANs for improved quality, stability, and variation. In: International conference on learning representations. https://openreview.net/forum?id=Hk99zCeAb
27. Isola P, Zhu J, Zhou T, Efros AA (2017) Image-to-image translation with conditional adversarial networks. In: 2017 IEEE conference on computer vision and pattern recognition (CVPR), pp 5967–5976. https://doi.org/10.1109/CVPR.2017.632
28. Zhu J, Park T, Isola P, Efros AA (2017) Unpaired image-to-image translation using cycle-consistent adversarial networks. In: 2017 IEEE international conference on computer vision (ICCV), pp 2242–2251. https://doi.org/10.1109/ICCV.2017.244
29. Kim T, Park E, Lee H, Moon Y-J, Bae S-H, Lim D, Jang S, Kim L, Cho I-H, Choi M, Cho K-S (2019) Solar farside magnetograms from deep learning analysis of stereo/euvi data. Nat Astron 3(5):397–400. https://doi.org/10.1038/s41550-019-0711-5
30. Park E, Moon Y-J, Lee J-Y, Kim R-S, Lee H, Lim D, Shin G, Kim T (2019) Generation of solar UV and EUV images from SDO/HMI magnetograms by deep learning. Astrophys J 884(1):23. https://doi.org/10.3847/2041-8213/ab46bb

31. Wang T-C, Liu M-Y, Zhu J-Y, Tao A, Kautz J, Catanzaro B (2018) High-resolution image synthesis and semantic manipulation with conditional gans. In: Proceedings of the IEEE conference on computer vision and pattern recognition
32. Del Zanna G, Mason HE (2018) Solar uv and x-ray spectral diagnostics. Liv Rev Sol Phys 15(1):5. https://doi.org/10.1007/s41116-018-0015-3
33. Galvez R, Fouhey DF, Jin M, Szenicer A, Munoz-Jaramillo A, Cheung MCM, Wright PJ, Bobra MG, Liu Y, Mason J, Thomas R (2019) A machine-learning data set prepared from the NASA solar dynamics observatory mission. Astrophys J Suppl Ser 242(1):7. https://doi.org/10.3847/1538-4365/ab1005
34. Shin G, Moon Y-J, Park E, Jeong H-J, Lee H, Bae S-H (2020) Generation of high-resolution solar pseudo-magnetograms from ca ii k images by deep learning. Astrophys J 895(1):16. https://doi.org/10.3847/2041-8213/ab9085
35. Jeong H-J, Moon Y-J, Park E, Lee H (2020) Solar coronal magnetic field extrapolation from synchronic data with AI-generated farside. Astrophys J 903(2):25. https://doi.org/10.3847/2041-8213/abc255
36. Lecun Y, Bottou L, Bengio Y, Haffner P (1998) Gradient-based learning applied to document recognition. Proc IEEE 86(11):2278–2324. https://doi.org/10.1109/5.726791
37. Ermolli I, Fofi M, Torelli M (1997) The Rome P.S.P.T. (Precision Solar Photometric Telescope): one year after. In: Hadjidemetrioy JD, Seiradakis JH (eds) Joint European and National astronomical meeting, p. 37
38. Choi Y, Choi M, Kim M, Ha J-W, Kim S, Choo J: Stargan: unified generative adversarial networks for multi-domain image-to-image translation. In: Proceedings of the IEEE conference on computer vision and pattern recognition (CVPR) (2018)
39. Ronneberger O, Fischer P, Brox T (2015) U-net: convolutional networks for biomedical image segmentation. In: Navab N, Hornegger J, Wells WM, Frangi AF (eds) Medical image computing and computer assisted intervention—MICCAI 2015. Springer, Cham, pp 234–241
40. Wang Z, Bovik AC, Sheikh HR, Simoncelli EP (2004) Image quality assessment: from error visibility to structural similarity. IEEE Trans Image Process 13(4):600–612. https://doi.org/10.1109/TIP.2003.819861

Terms and Conditions

Springer Nature journal content, brought to you courtesy of Springer Nature Customer Service Center GmbH ("Springer Nature").

Springer Nature supports a reasonable amount of sharing of research papers by authors, subscribers and authorised users ("Users"), for small-scale personal, non-commercial use provided that all copyright, trade and service marks and other proprietary notices are maintained. By accessing, sharing, receiving or otherwise using the Springer Nature journal content you agree to these terms of use ("Terms"). For these purposes, Springer Nature considers academic use (by researchers and students) to be non-commercial.

These Terms are supplementary and will apply in addition to any applicable website terms and conditions, a relevant site licence or a personal subscription. These Terms will prevail over any conflict or ambiguity with regards to the relevant terms, a site licence or a personal subscription (to the extent of the conflict or ambiguity only). For Creative Commons-licensed articles, the terms of the Creative Commons license used will apply.

We collect and use personal data to provide access to the Springer Nature journal content. We may also use these personal data internally within ResearchGate and Springer Nature and as agreed share it, in an anonymised way, for purposes of tracking, analysis and reporting. We will not otherwise disclose your personal data outside the ResearchGate or the Springer Nature group of companies unless we have your permission as detailed in the Privacy Policy.

While Users may use the Springer Nature journal content for small scale, personal non-commercial use, it is important to note that Users may not:

1. use such content for the purpose of providing other users with access on a regular or large scale basis or as a means to circumvent access control;
2. use such content where to do so would be considered a criminal or statutory offence in any jurisdiction, or gives rise to civil liability, or is otherwise unlawful;
3. falsely or misleadingly imply or suggest endorsement, approval , sponsorship, or association unless explicitly agreed to by Springer Nature in writing;
4. use bots or other automated methods to access the content or redirect messages
5. override any security feature or exclusionary protocol; or
6. share the content in order to create substitute for Springer Nature products or services or a systematic database of Springer Nature journal content.

In line with the restriction against commercial use, Springer Nature does not permit the creation of a product or service that creates revenue, royalties, rent or income from our content or its inclusion as part of a paid for service or for other commercial gain. Springer Nature journal content cannot be used for inter-library loans and librarians may not upload Springer Nature journal content on a large scale into their, or any other, institutional repository.

These terms of use are reviewed regularly and may be amended at any time. Springer Nature is not obligated to publish any information or content on this website and may remove it or features or functionality at our sole discretion, at any time with or without notice. Springer Nature may revoke this licence to you at any time and remove access to any copies of the Springer Nature journal content which have been saved.

To the fullest extent permitted by law, Springer Nature makes no warranties, representations or guarantees to Users, either express or implied with respect to the Springer nature journal content and all parties disclaim and waive any implied warranties or warranties imposed by law, including merchantability or fitness for any particular purpose.

Please note that these rights do not automatically extend to content, data or other material published by Springer Nature that may be licensed from third parties.

If you would like to use or distribute our Springer Nature journal content to a wider audience or on a regular basis or in any other manner not expressly permitted by these Terms, please contact Springer Nature at

onlineservice@springernature.com